INTERFACE ELEMENTS IN GEOTECHNICAL ENGINEERING – SOME NUMERICAL ASPECTS AND APPLICATIONS

Rafael C. Barros

Luma A. C. de Vasconcelos

Christianne L. Nogueira

Ricardo A. M. Silveira

rafaelcesario@hotmail.com

luma-alvarenga@hotmail.com

clnogueira2015@yahoo.com.br

ramsilveira@yahoo.com.br

Universidade Federal de Ouro Preto

Campus Morro do Cruzeiro, 35400-000, Ouro Preto, Minas Gerais, Brazil

Abstract. *The purpose of this paper is to present a null thickness interface element with nonlinear constitutive behavior to be used under plane strain and axi-symmetric conditions. In order to emphasize the capabilities of this element two categories of examples are evaluated. The patch test examples category aims to investigate the interface elements formulations and stress integration algorithm and the field problem category involves a long block under a rigid foundation analysis. In these cases the implementation is verified when compared to some analytical problems. A study of its kinetic inconsistency, ill-conditioning, and numerical integration are also provided.*

Keywords: *Null thickness interface elements, elastic perfectly plastic constitutive model, pullout test.*

1 INTRODUCTION

Interface elements are used to represent the contact between bodies with dissimilar materials allowing simulation of relative movements between them. In geotechnical engineering, they are used to represent: joints in fractured rock, soil-structure interactions in foundation and earth retaining problems (Goodman et al., 1968; Ghaboussi et al, 1973; Heuze and Barbour, 1982; Plesha, 1987; Day and Potts, 1994 and 1998; Boulon et al, 1995; Mao, 2004) and recently the soil- reinforcement interaction in reinforced soil structures (Sugimoto and Alagiyawanna, 2003; Wang and Wang, 2006).

In general, interface elements can be divided into two categories. The first is null thickness elements (Goodman et al., 1968; Beer, 1985; Gens et al., 1998; Day and Potts, 1994 and 1998; Kaliakin and Li, 1995; Lei, 2001; Bouzid at al., 2004) and the second is tiny thickness elements (Pande and Sharma, 1979; Desai et al., 1984; Wang and Wang, 2002; Wang and Wang, 2006). There are many formulations of both categories to be found in the literature.

The purpose of this paper is to present a null thickness interface element with nonlinear constitutive behavior to be used under plane strain and axi-symmetric conditions. In order to emphasize the capabilities of this element, examples are provided that include a study of its kinetic inconsistency, ill-conditioning, and numerical integration.

2 FORMULATION

Figure 1a depicts a generic discontinuity on a generic body. Figure 1b presents general discontinuity segment. This general segment is positioned trough the x´ longitudinal direction oriented by the β angle related to the horizontal direction x. The discontinuity segment is defined by its top (t) and bottom (b) faces which can displace on longitudinal (s) and normal (*n*) direction. The longitudinal displacement of top and bottom faces are identified, respectively, by v'_t and v'_b. On the other hand, normal displacement of top and bottom faces are identified, respectively, by u'_t and u'_b. Also, Fig. 1b presents the positive direction of the normal (σ) and shear (τ) stresses trough the discontinuity segment.

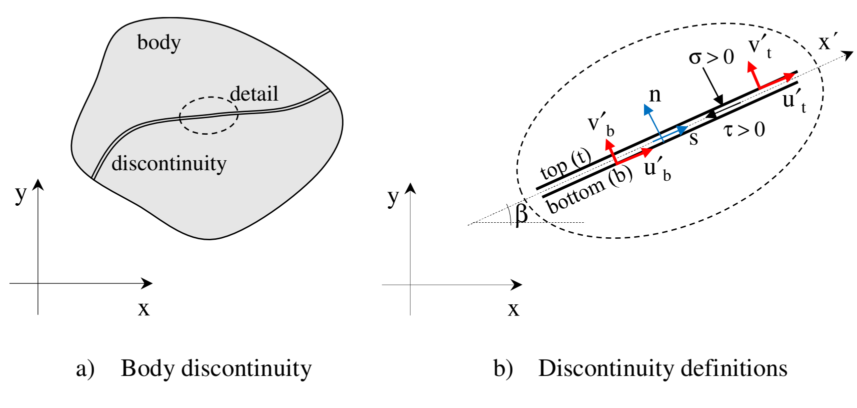

a) Body discontinuity b) Discontinuity definitions

Figure 1. Body discontinuity

Figure 2 illustrates the discontinuity's movement modes in terms of the longitudinal (δ_s) and the normal (δ'_n) relative displacement vector (δ') defined as:

$$\delta' = \begin{Bmatrix} \delta'_s \\ \delta'_n \end{Bmatrix} = -\begin{Bmatrix} u'_t - u'_b \\ v'_t - v'_b \end{Bmatrix} \tag{1}$$

During an opening process ($\delta'_n < 0$) a tension normal stress ($\sigma < 0$) is developed on the discontinuity while during a closing process ($\delta'_n > 0$) a compressive normal stress ($\sigma > 0$) is developed on the discontinuity. In terms of the longitudinal relative displacement (δ'_s), when the top face slides over the bottom face ($\delta'_s < 0$) a negative shear stress ($\tau < 0$) is observed on the s positive direction. On the other hand, when the bottom face slides overs the top face $(\delta'_s > 0)$ positive shear stress ($\tau > 0$) is observed on the s negative direction.

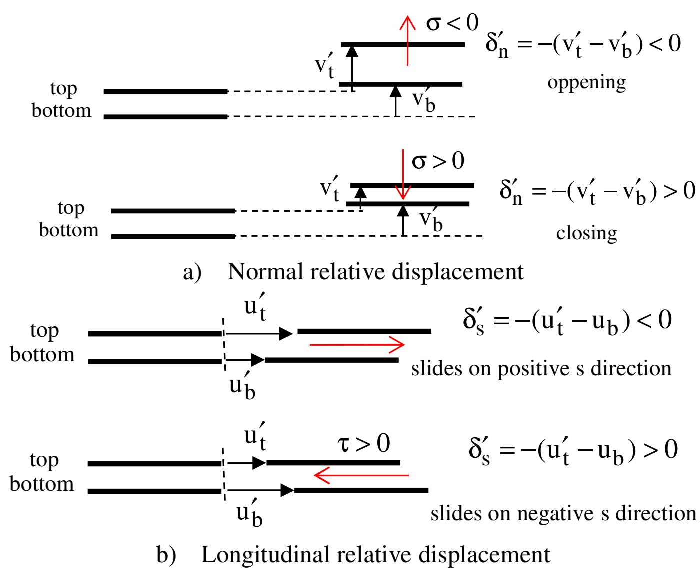

Figure 2. Movement modes

The interface constitutive model adopted is linear elastic in terms of the normal stress and non-associate, without hardening and elastic perfectly plastic in terms of the shear stress. The constitutive relationship between the normal stress (σ) and normal relative displacement (δ'_n) is presented in Fig. 3a in which k_n is the normal stiffness by unity area. The minimal normal stress which can occur through the interface is defined as σ^F_{min} which is illustrated on Fig. 4. The constitutive relationship between the shear stress (τ) and shear relative displacement (δ'_s) is presented in Fig. 3b in which k_s is the shear stiffness by unity area and τ_{max} is the interface slip (or shear) strength which is illustrated on Fig. 4.

The interface slip strength is defined by the Mohr-Coulomb criteria (Fig. 4) which is used as the yield function (F). By adopting a non-associate plasticity concept the yield function (F) and the plastic potential function (G) can be written as:

$$F = |\tau| - c - \sigma\, tg\varphi = 0 \tag{2a}$$

$$G = |\tau| - c - \sigma \, tg\psi = 0 \tag{2b}$$

where c is the cohesion, ϕ is the frictional angle and ψ is the dilatancy angle.

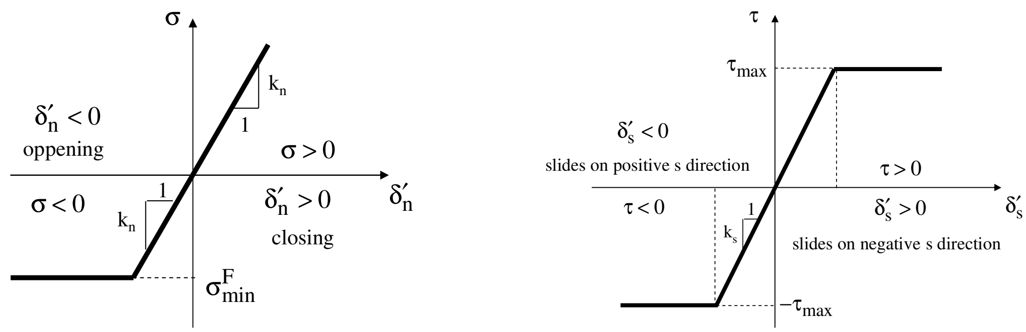

a) Linear elastic b) Elastic perfectly plastic

Figure 3. Idealized constitutive behavior

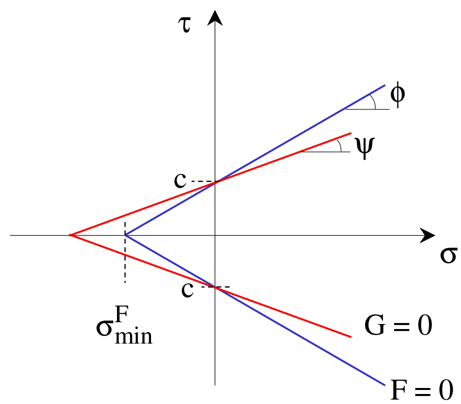

Figure 4. Yield and potential plastic functions

According to the Fig. 4, the minimal normal stress is defined as:

$$\sigma^F_{min} = c \cot an(\phi) \tag{3a}$$

and the maximal shear strength is given by:

$$\tau_{max} = c + \sigma \tan \phi \tag{3b}$$

This discontinuity segment presented in Fig. 1b, can be modeled by FEM by adopting interface elements based on the null thickness interface element given by Goodman et al. (1968) as presented in Fig. 5.

a) Linear interface element (J4) b) Quadratic interface element (J6)

Figure 5. Interface element

Using the concept of isoparametric formulation, the longitudinal coordinate (x´) of any point into the element is given by:

$$\mathbf{x}' = \mathbf{NT}\hat{\mathbf{x}} \tag{4}$$

where

$$\hat{\mathbf{x}}^T = \begin{bmatrix} x_1 & y_1 & \ldots & x_{nnoel/2} & y_{nnoel/2} \end{bmatrix} \tag{5}$$

is the nodal local coordinate vector:

$$\mathbf{N} = \begin{bmatrix} N_1 & \cdots & N_{nnoel/2} \end{bmatrix} \tag{6}$$

is the shape function matrix that contains the interpolation functions N_i which depends on the element. For the J4 element (Figure 5a), the interpolation functions are defined as:

$$N_1 = 0.5(1-r) \tag{7a}$$

$$N_2 = 0.5(1+r) \tag{7b}$$

and, for the J6 elements (Fig. 5b), they are defined as:

$$N_1 = 0.5(r^2 - r) \tag{8a}$$

$$N_2 = (1 - r^2) \tag{8b}$$

$$N_3 = 0.5(r^2 + r) \tag{8c}$$

the coordinate transformation matrix **T** is defined as:

$$\mathbf{T} = \begin{bmatrix} \cos\beta & \sin\beta & 0 & 0 & 0 & 0 \\ \vdots & \vdots & \cdots & \cdots & \vdots & \vdots \\ 0 & 0 & 0 & 0 & \cos\beta & \sin\beta \end{bmatrix} \tag{9}$$

where

$$\cos\beta = \frac{dx/dr}{\det J} \tag{10a}$$

$$\sin\beta = \frac{dy/dr}{\det J} \tag{10b}$$

$$\det J = \sqrt{\left(\frac{dx}{dr}\right)^2 + \left(\frac{dy}{dr}\right)^2} \tag{10c}$$

The relative displacement vector ($\boldsymbol{\delta}'$) is defined in terms of the shear (δ'_s) and normal (δ'_n) relative displacement between the bottom and top element's face by doing:

$$\boldsymbol{\delta}' = \begin{Bmatrix} \delta'_s \\ \delta'_n \end{Bmatrix} = -\begin{Bmatrix} u'_t - u'_b \\ v'_t - v'_b \end{Bmatrix} = \mathbf{B}\,\mathbf{T}_B\,\hat{\mathbf{u}} \tag{11}$$

where

$$\hat{\mathbf{u}}^T = \begin{bmatrix} u_1 & v_1 & \ldots & u_{nnoel} & v_{nnoel} \end{bmatrix} \tag{12}$$

is the local nodal displacement vector related to the local coordinate system; **B** is the cinematic matrix defined as a function of the interpolation function as:

$$\mathbf{B} = \begin{bmatrix} N_1 & 0 & \cdots & N_{nnoel/2} & 0 & -N_{nnoel/2} & 0 & \cdots & -N_1 & 0 \\ 0 & N_1 & \cdots & 0 & N_{nnoel/2} & 0 & -N_{nnoel/2} & \cdots & 0 & -N_1 \end{bmatrix} \tag{13}$$

and

$$\mathbf{T}_B = \begin{bmatrix} \cos\beta & \sin\beta & \cdots & 0 & 0 \\ \cos\beta & \sin\beta & \cdots & 0 & 0 \\ \vdots & \vdots & \ddots & \vdots & \vdots \\ 0 & 0 & \cdots & \cos\beta & \sin\beta \\ 0 & 0 & \cdots & \cos\beta & \sin\beta \end{bmatrix} \tag{14}$$

Due to the non-linear nature of the elastic plastic mechanical problem, the equilibrium equation is solved, starting from a given equilibrium configuration n, by adopting an incremental-iterative procedure where at the end of each loading step states variables are updated. In this strategy, the problem solution is obtained by updating the nodal displacement vector ($\hat{\mathbf{U}}$) in each new equilibrium configuration, by doing:

$$\hat{\mathbf{U}}_{n+1} = \hat{\mathbf{U}}_n + \boldsymbol{\Delta}\hat{\mathbf{U}} \tag{15}$$

where $\hat{\mathbf{U}}_n$ is the global nodal displacement vector at the beginning of each load step and

$$\boldsymbol{\Delta}\hat{\mathbf{U}} = \boldsymbol{\Delta}\hat{\mathbf{U}}^0 + \sum_{k=1}^{iter} \delta\boldsymbol{\Delta}\hat{\mathbf{U}}^k \tag{16}$$

is the incremental global nodal displacement vector which is obtained by correcting the incremental predict solution ($\boldsymbol{\Delta}\hat{\mathbf{U}}^0$) by successive iteration ($\delta\boldsymbol{\Delta}\hat{\mathbf{U}}$) until reaching a new equilibrium configuration n+1. The number of iterative cycle (iter) necessary to obtain the convergence is not known. So a maximal number of iterative cycles are provided in order to guarantee the procedure convergence at the current step.

The incremental predict solution is obtained by doing:

$$\boldsymbol{\Delta}\hat{\mathbf{U}}^0 = \left[\mathbf{K}_{ep}\right]^{-1} \Delta\lambda\mathbf{F}_{ext} \tag{17}$$

where K_{ep} is the global stiffness matrix that represents the global arrangement of the element stiffness matrix K^e given, for plane strain condition, by:

$$\mathbf{K}^e = \int_{-1}^{+1} \left[(\mathbf{BT}_B)^T \mathbf{D}_{ep} (\mathbf{BT}_B) \right] \det \mathbf{J} dr \tag{18a}$$

or, for axi-symmetric condition, as:

$$\mathbf{K}^e = \int_{-1}^{+1} \left[(\mathbf{BT}_B)^T \mathbf{D}_{ep} (\mathbf{BT}_B) \right] (2\pi x') \det \mathbf{J} dr \tag{18b}$$

where

$$\mathbf{D}_{ep} = \mathbf{D}_e - \mathbf{D}_p \tag{19}$$

is the elastoplastic constitutive matrix that contains two parcels, one elastic parcel:

$$\mathbf{D}_e = \begin{bmatrix} k_s & 0 \\ 0 & k_n \end{bmatrix} \tag{20a}$$

and one plastic parcel (Brocklehurst,1993):

$$\mathbf{D}_p = \frac{1}{k_s + k_n \operatorname{tg}\theta \operatorname{tg}\psi} \begin{bmatrix} k_s^{\,2} & k_n k_s \operatorname{signal}(\tau) \operatorname{tg}\varphi \\ k_n k_s \operatorname{signal}(\tau) \operatorname{tg}\psi & k_n^{\,2} \operatorname{tg}\varphi \operatorname{tg}\psi \end{bmatrix} \tag{20b}$$

The vector $\mathbf{F}_{ext}$ represents the external nodal force applied at each load step and kept constant throughout the iterative cycles, according to the Newton-Raphson iterative scheme. This vector is updated at the beginning of a given step load by:

$$\mathbf{F}_{ext} = \mathbf{F}_{ext\,n} + \Delta\lambda \mathbf{F}_{ext} \tag{21}$$

where $\mathbf{F}_{ext\,n}$ is the external nodal force vector at a given equilibrium configuration n. In Equation (16) $\Delta\lambda$ is the increment of load factor, which can be automatically, defined starting from the initial trial provided by the user (Nogueira 1998; Oliveira 2006; Simão 2014).

The iterative solution is obtained by doing:

$$\delta\Delta\hat{\mathbf{U}}^k = \left[\mathbf{K}_{ep} \right]^{-1} \boldsymbol{\psi}^k \tag{22}$$

in which:

$$\boldsymbol{\psi}^k = \mathbf{F}_{ext} - \mathbf{F}_{int}^{\;k} \tag{23}$$

is the unbalanced force vector at the iterative cycle k and $\mathbf{F}_{int}^{\;k}$ represents the global arrangement of the element internal nodal force vector $\mathbf{F}_{int}^{e\;k}$ defined, for plane strain condition, as:

$$\mathbf{F}_{int}^{e\;k} = \int_{-1}^{+1} (\mathbf{BT}_B)^T \boldsymbol{\sigma}^k \det \mathbf{J} dr \tag{24a}$$

or, for axi-symmetric condition, as:

$$\mathbf{F}_{int}^{e\ k} = \int_{-1}^{+1} \left(\mathbf{B}\mathbf{T}_B\right)^T \boldsymbol{\sigma}^k (2\pi x') \det \mathbf{J} dr \tag{24b}$$

The stress state vector $\boldsymbol{\sigma}^k$ is evaluated on each iterative cycle by doing:

$$\boldsymbol{\sigma}^k = \begin{Bmatrix} \tau \\ \sigma \end{Bmatrix} = \boldsymbol{\sigma}_n + \Delta\boldsymbol{\sigma}^k \tag{25}$$

where

$$\Delta\boldsymbol{\sigma}^k = \mathbf{D}_{ep}\left(\mathbf{B}\,\mathbf{T}_B\right)\Delta\hat{\mathbf{u}} \tag{26}$$

$\Delta\hat{\mathbf{u}}$ is the incremental displacement vector at element level and updated at the current iterative cycle.

At the end of each iterative cycle, a convergence state of the solution is verified by using a criterion that relates the Euclidian norm of the unbalance nodal force vector with the Euclidian norm of the external nodal force vector. Thus, for a given tolerance and at each increment, the iterative scheme ensures the overall balance by satisfying the compatibility conditions, boundary conditions and constitutive relationships.

As the iterative scheme involves the stress state evaluation at each iterative cycle, a stress integration algorithm must be used in order to guarantee the consistency condition related to elastoplastic models. The stress integration algorithm adopted in this paper is presented in Fig. 6. This algorithm considers five situations which can occur on each loading step:

Situation (i): the stress state at the beginning of the current loading step ($\boldsymbol{\sigma}_n$) is initially inside the yield surface ($F(\boldsymbol{\sigma}_n) < 0$), and the elastic predictor stress ($\boldsymbol{\sigma}^*_{n+1}$) continues inside the yield surface ($F(\boldsymbol{\sigma}^*_{n+1}) < 0$).

Situation (ii): the stress state at the beginning of the current loading step ($\boldsymbol{\sigma}_n$) is initially inside the yield surface ($F(\boldsymbol{\sigma}_n) < 0$), and the elastic predictor reaches the yield surface $\left(F(\boldsymbol{\sigma}^*_{n+1}) = 0\right)$.

Situation (iii): the stress state at the beginning of the current loading step ($\boldsymbol{\sigma}_n$) is initially on the yield surface ($F(\boldsymbol{\sigma}_n) = 0$), and the elastic predictor goes beyond the yield surface $\left(F(\boldsymbol{\sigma}^*_{n+1}) > 0\right)$. In this case, the stress increment is purely plastic and the stress vector must be reevaluated using the elastoplastic matrix ($\mathbf{D}_{ep}$);

Situation (iv): the stress state at the beginning of the current loading step ($\boldsymbol{\sigma}_n$) is initially inside the yield surface ($F(\boldsymbol{\sigma}_n) < 0$), and the elastic predictor goes beyond of the yield surface ($F(\boldsymbol{\sigma}^*_{n+1}) > 0$). In this case there is a transition from elastic to plastic state. So a scalar (α) should be evaluated to define the elastic portion of the deformation increment ($\alpha d\boldsymbol{\delta}'$).

Situation (v): the stress state at the beginning of the current loading step ($\boldsymbol{\sigma}_n$) is initially inside the yield surface ($F(\boldsymbol{\sigma}_n) < 0$), and the elastic predictor reaches a stress state in which

Proceedings of the XXXVIII Iberian Latin-American Congress on Computational Methods in Engineering
P.O. Faria, R.H. Lopez, L.F.F. Miguel, W.J.S. Gomes, M. Noronha (Editores), ABMEC, Florianópolis, SC, Brazil, November 5-8, 2017.

normal stress is less than $c \cot g\varphi$. In this case there is contact loss and the stress vector must be set at null ($\tau = \sigma = 0$).

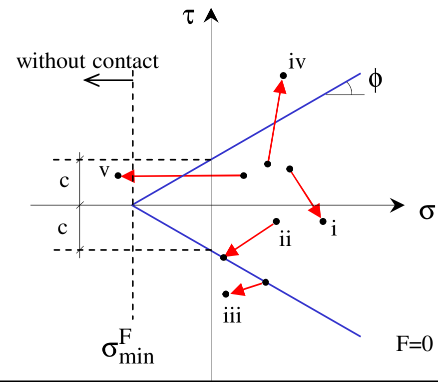

(1) Knowing: $\boldsymbol{\sigma}_n$ and $d\boldsymbol{\delta}'$! $FTOL \approx 10^{-10}$

(2) Evaluate: $F(\boldsymbol{\sigma}^*_{n+1})$ where $\boldsymbol{\sigma}^*_{n+1} = \boldsymbol{\sigma}_n + \mathbf{D}_e d\boldsymbol{\delta}'$

(3) Verifies the contact loose:

If $\sigma^*_{n+1} \leq -c \cot \varphi$ then do $\sigma_{n+1} = \tau_{n+1} = 0$ and quit !Situation v

(4) If $F(\boldsymbol{\sigma}^*_{n+1}) \leq FTOL$ then do $\boldsymbol{\sigma}_{n+1} = \boldsymbol{\sigma}^*_{n+1}$ and quit !Situations i and ii

(5) If $|F(\boldsymbol{\sigma}_n)| \leq$ FTOL then do $\boldsymbol{\sigma}_{n+1} = \boldsymbol{\sigma}_n + \mathbf{D}_t(\boldsymbol{\sigma}_n) d\boldsymbol{\delta}'$ and quit !Situation iii

(6) If $F(\boldsymbol{\sigma}_n) <$ -FTOL !Situation iv

Evaluate α doing $|F(\boldsymbol{\sigma}_n + \alpha \mathbf{D}_e d\boldsymbol{\delta}')| \leq FTOL$!

Evaluate: $\boldsymbol{\sigma}^*_{n+1} = \boldsymbol{\sigma}_n + \alpha \mathbf{D}_e d\boldsymbol{\delta}'$

Update $\boldsymbol{\sigma}_{n+1} = \boldsymbol{\sigma}_n + (1-\alpha)\mathbf{D}_t(\boldsymbol{\sigma}^*_{n+1}) d\boldsymbol{\delta}'$ and quit

Figure 6. Constitutive behavior during some loading path (Oliveira 2006)

3 VERIFICATION EXAMPLES

Different examples are shown in this section. These are used to verify the implementation of the interface element into ANLOG program (Pereira, 2003 and Oliveira, 2006). Two categories of examples are presented in this paper and are illustrated into Fig. 7 and 8.

Figure 7 presents the patch test examples category in which the interface elements formulations and stress integration algorithm are investigated. The numerical integration's influence is analyzed and the stress integration scheme to elastoplastic interface under axi-symmetric condition. This example investigates the interface element capability of predicting correctly the stress through the interface under different deformation paths.

Figure 8 presents the field problem example category in plane strain. The example is a long elastic block sliding between two rigid, but top smooth and bottom rough, surfaces. The numerical results are compared to the analytical solution presented.

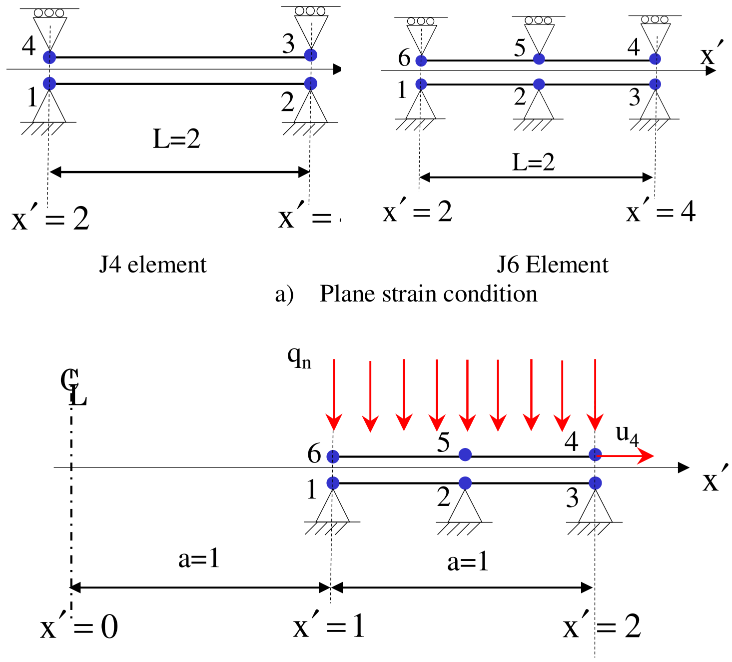

a) Plane strain condition

b) Stress integration test for axi-symmetric condition

Figure 7. Patch test

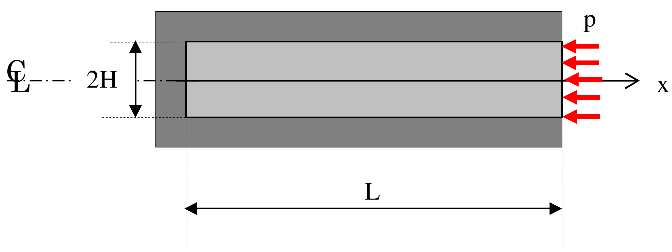

Figure 8. Field problem - long elastic block

3.1 Example 1 – interface elements under plane strain condition

In this item a generic interface between two bodies with length (L) equal 2 and placed horizontally (β=0) is analyzed under plane strain condition. The linear (J4) and quadratic (J6) interface element presented in Fig. 7a is used by considering a linear elastic constitutive model with shear stiffness by unity area (k_s) is equal to 1. As the nodal vertical displacements are fixed only the shear behavior is analyzed in this example.

Table 1 presents the reduced stiffness matrix (without taking into account the column and line related to the degree of freedom of the nodes 1 and 2 which are fixed and both direction and the nodes 3 and 4 for in a vertical direction) for these elements obtained by analytical and numerical integration. Different numerical integration schemes are used to investigate the kinetic inconsistency described by several authors (Schellekens and De Borst, 1993; Gens, et *a*l., 1995; Coutinho et al*.*, 2003).

Table 1. Stiffness matrix

Elem.	Analytical	Numerical Integration		
		ng	Gauss-Legendre (GL)	Gauss Lobato (GLb)
J4	$\begin{bmatrix} 2/3 & 1/3 \\ 1/3 & 2/3 \end{bmatrix}$	2	$\begin{bmatrix} 2/3 & 1/3 \\ 1/3 & 2/3 \end{bmatrix}$	$\begin{bmatrix} 1 & 0 \\ 0 & 1 \end{bmatrix}$
		3	$\begin{bmatrix} 2.921/4 & 1/3 \\ 1/3 & 2.921/4 \end{bmatrix}$	$\begin{bmatrix} 2/3 & 1/3 \\ 1/3 & 2/3 \end{bmatrix}$
J6	$\begin{bmatrix} 4/15 & 2/15 & -1/15 \\ 2/15 & 16/15 & 2/15 \\ -1/15 & 2/15 & 4/15 \end{bmatrix}$	2	$\begin{bmatrix} 2/9 & -2/9 & -1/9 \\ 2/9 & 8/9 & 2/9 \\ -1/9 & 2/9 & 2/9 \end{bmatrix}$	$\begin{bmatrix} 1 & 0 & 0 \\ 0 & 0 & 0 \\ 0 & 0 & 1 \end{bmatrix}$
		3	$\begin{bmatrix} 4/15 & 2/15 & -1/15 \\ 2/15 & 16/15 & 2/15 \\ -1/15 & 2/15 & 4/15 \end{bmatrix}$	$\begin{bmatrix} 1/3 & 0 & 0 \\ 0 & 4/3 & 0 \\ 0 & 0 & 1/3 \end{bmatrix}$

ng = number of numerical integrations

As one can see on Table 1, for the J4 element the numerical integration of Gauss Legender adopting tow Gauss points leads to a numerical stiffness matrix equal to the analytical one. For this element, the Gauss Lobato numerical scheme must adopt three Gauss point in order to achieve the analytical response for the stiffness matrix. On the other hand, for the J6 element the numerical integration of Gauss Legender adopting three Gauss points leads to a numerical stiffness matrix equal to the analytical one. For this element, the Gauss Lobato numerical scheme does not provide a good approximation for the analytical stiffness matrix. So the authors recommend the use of Gauss-Legender numerical integration by adopting two integration points for the J4 element and three integration points for the J6 element.

By considering the stiffness matrix presented in Table 1, the J4 and J6 interface elements were analyzed under different loading conditions as illustrated in Tables 2 and 3. Even been a linear elastic constitutive problem, the internal force (Eq. 24) is evaluated by considering only the elastic parcel of the constitutive matrix (Eq. 20a) used on the stress state calculation (Eq. 26). This strategy was adopted only to verify if the displacement results leads to a self-balanced stress state.

The results presented in Tables 2 and 3 point out that there are kinetic inconsistency and oscillatory behavior in terms of the shear stress through the interface and this is related with the loading condition (Coutinho et al., 2003). When the nodal force applied represents the equivalent force to uniform shear stress through the interface (Case H3 to J4 element and H4 to J6 element) there are no kinds of inconsistency. The loading conditions H1 and H2 to J4 element and H1, H2 and H3 to J6 element provides a oscillatory behavior in terms of the shear stress but are self-balanced and do not lead a problem when used in a finite element mesh with other plane elements.

Table 2. Simple Tests– J4 Element

Load case	External force		Displacement		Shear Stress		Internal Force	
	$F_{ex\ 4}$	$F_{ex\ 3}$	u_4	u_3	τ_1	τ_2	$F_{in\ 4}$	$F_{in\ 3}$
H1	1	0	2	-1	1.366	-0.366	1	0
H2	0	1	-1	2	-0.366	1.366	0	1
H3	1	1	1	1	1	1	1	1

Table 3. Simple Tests – J6 Element

Load Case	External force			Displacement			Shear stress			Internal force		
	$F_{ex\ 6}$	$F_{ex\ 5}$	$F_{ex\ 4}$	u_6	u_5	u_4	τ_1	τ_2	τ_3	$F_{in\ 6}$	$F_{in\ 5}$	$F_{in\ 4}$
H1	1	0	0	4.5	-0.75	1.5	2.662	-0.75	0.338	1	0	0
H2	0	1	0	-0.75	1.125	-0.75	0	1.125	0	0	1	0
H3	0	0	1	1.5	-0.75	4.5	0.338	-0.75	2.662	0	0	1
H4	1/3	4/3	1/3	1	1	1	1	1	1	1/3	4/3	1/3

3.2 Example 2 – interface elements in axi-symmetric condition

An axi-symmetric interface element is illustrated in Fig. 7b(Oliveira et al 2005). The bottom face of the interface element is fixed in both directions (axial and radial) while the top face of the element is submitted to a uniform normal surface load q_n (of a magnitude 100kPa) in order to produce an initial normal stress as the same magnitude. After that, a shear movement (u_4) is applied at the element top according to the following deformation path: shear path1 from 0.0 to +0.010m (Δu_4=+0.010m); shear path2 from +0.01m to +0.006m (Δu_4=-0.004m); shear path 3 from +0.006m to +0.012m (Δu_4=0.006m).

The geometric and boundary (in terms of displacement and force) conditions are shown in Fig. 7b. The following constitutive properties were adopted: $k_s=10^4$kN/m^3; c=0.0; $\phi=30^o$; and, ψ e k_n variables.

The path stress and the failure surface are presented in Fig. 9 adopting a null dilatancy angle and varying the normal stiffness. As one can see, the normal stiffness magnitude there is no influence of the stress path. The shear relative displacement imposed generates a simple shear path represented by the vertical part of the full path. The first horizontal stress path part represents the normal compression applied before the shear relative displacement. The negative value of the shear stress is in accordance with the signal convention adopted which is described in Fig. 2.

The normalized stress ($-\tau/\sigma$) versus normalized shear relative displacement ($-\delta_s/a$) is shown in Fig. 10 also by varying the dilatancy angle and the normal stiffness. According to results plotted in this figure the dilatancy angle doesn't influence the maximal shear stress level. It can be observed, also, the proportionality between shear stress and shear relative displacement is preserved during the shear deformation path. For a null dilatancy material there is no influence of the normal stiffness magnitude. However, for no null dilatancy angle material the magnitude of the normal stiffness affects the iterative process. For normal stiffness magnitude higher than the shear stiffness, no convergence is achieved in the iterative process and the ANLOG stops before the shear relative displacement on the loading path is completed.

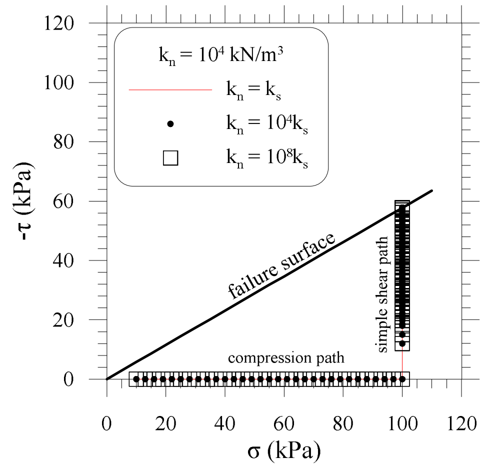

Figure 9. Path stress and failure surface

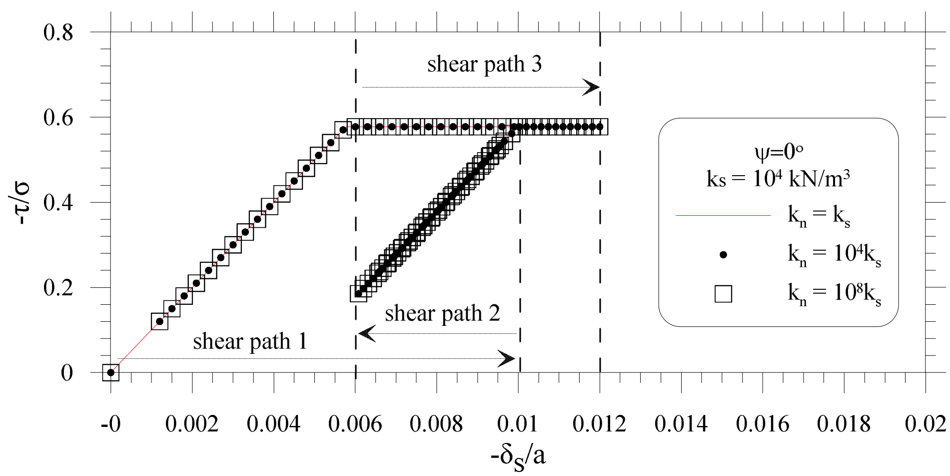

a) $\psi=0^o$ and k_n variable

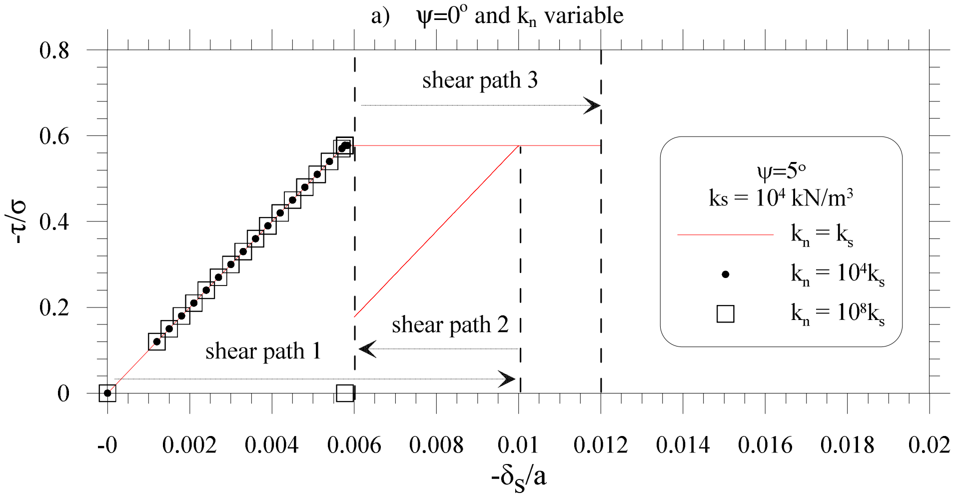

b) $\psi=5^o$ and k_n variable

Figure 10. Normalized stress and shear relative displacement – during the simple shear path

The influence of the dilatancy effect can be observed in Fig. 11 in terms of the normalized normal relative displacement (δ_n/a) and shear relative displacement (δ_s/a). During the simple shear path, no normal relative displacement is observed when the dilatancy angle in done null. The normal relative displacement, during the normal compression path depends on the normal stiffness magnitude as was expected.

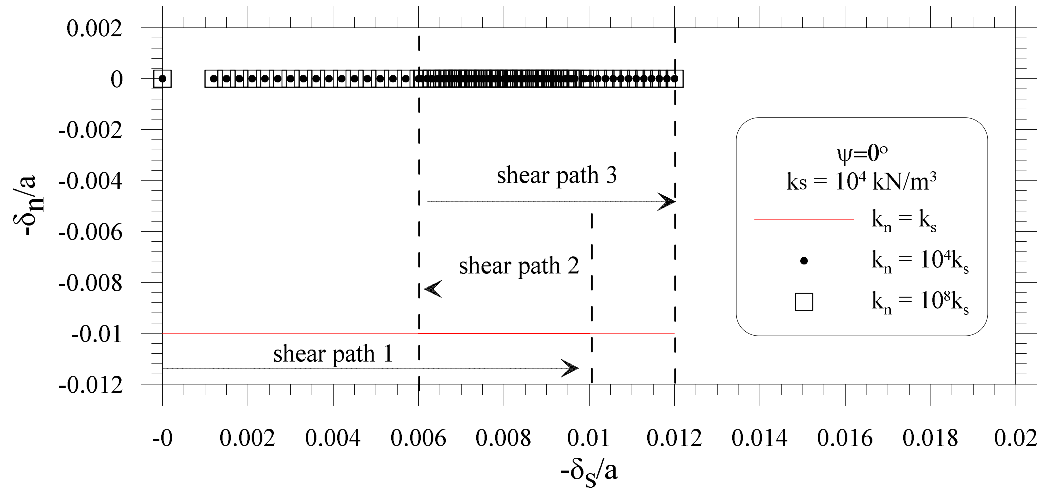

a) ψ=0° and k_n variable

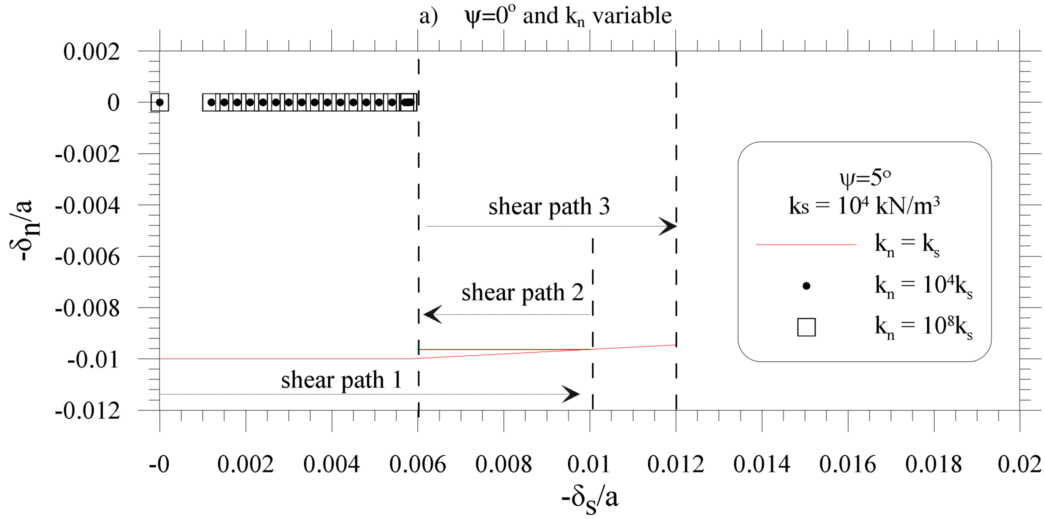

b) ψ=5° and k_n variable

Figure 11. Normalized shear displacement and normal displacement - – during the simple shear path

3.3 Example 3 – long elastic block

In this example, an elastic long block lays over a rigid foundation. An interface element is used to simulate the contact between the block and rigid foundation. The block is submitted to a compression force per unit length P on the right vertical face while the left vertical face is fixed (Fig. 8a). The FEM mesh with 12 quadrilateral quadratic isoparametric element (Nogueira 2010; Pereira 2003) and 12 J6 elements are presented in Fig. 12.

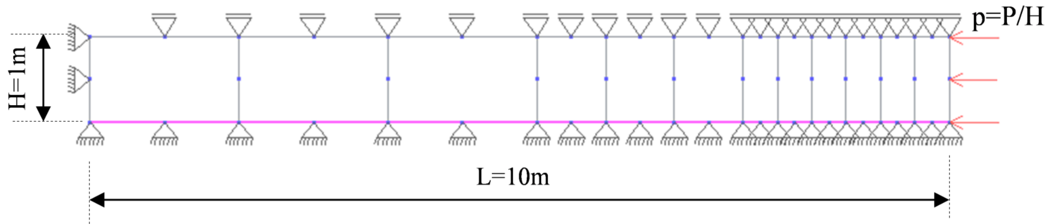

Figure 12. Long elastic block lain on rigid contact – FEM discretization

In this figure are indicated the boundary conditions in terms of displacement and force. The block elements are considered linear and elastic material with the following properties: E=100MPa and ν=0.0. The interface elements are modeled as an elastic perfectly plastic material with the following properties: c=30kPa; ϕ and ψ are variables; k_s=10MN/m^3; and k_n is variable.

The second order ordinay differential equation which represents this problem is given by (Hird and Russell 1990) in terms of the relative shear displacement in the interface (δ_s) as:

$$\frac{d^2\delta_s}{dx^2} - \alpha^2\delta_s = 0 \tag{27}$$

where

$$m_v = \frac{(1+\nu)(1-2\nu)}{E(1-\nu)} \tag{28}$$

$$\alpha = \sqrt{\frac{k_s m_v}{H}} \tag{29}$$

The analytical solution of the Eq. (27) is given by:

$$\delta_s(x) = C_1 e^{\alpha x} + C_2 e^{-\alpha x} \tag{30}$$

Considering the shear relative displacement null at the fixed boundary condition in x=0, one can obtain:

$$\delta_s(x) = C\left(e^{\alpha x} - e^{-\alpha x}\right) \tag{31}$$

By applying the natural boundary condition is possible to obtain:

$$C = \left.\frac{d\delta_s}{dx}\right|_{x=x^*} \left[\frac{1}{\alpha\left(e^{\alpha x^*} + e^{-\alpha x^*}\right)}\right] \tag{32}$$

In the field of elasticity theory, considering a load level which is not going mobilize the shear strength of the interface, it is possible to states that x*=L, then:

$$\left.\frac{d\delta_s}{dx}\right|_{x=L} = m_v \left.\sigma_x\right|_{x=L} = \frac{m_v P}{H} \tag{33}$$

Then the analytical solution of the Eq. (1) for $x \in [0, L]$, is given by

$$\delta_s(x) = \frac{m_v P}{\alpha H}\left(\frac{e^{\alpha x} - e^{-\alpha x}}{e^{\alpha L} + e^{-\alpha L}}\right) \tag{34}$$

Equations (34a) and (34b), however is valid only for shear stress level lower than the shear strength through the interface (τ_{max}) defined, for a pure cohesive material ($\phi = \psi = 0^o$), as a function of the cohesion as:

$$\tau_{max} = c \tag{35}$$

As the shear stress on the interface increases with the level force *P*, it is important to define the point (x_1) up to it the shear stress reaches its maximal value. At this point the Eq. (33) is defined as:

$$\left.\frac{d\delta_s}{dx}\right|_{x=x_1} = m_v \left.\sigma_x\right|_{x=x_1} = m_v\left[\frac{P}{H} - \tau_{max}(L - x_1)\right] \tag{36}$$

Then the analytical solution of the Eq. (1) from x=0 to $x=x_1$ is given by:

$$\delta_s(x) = \frac{m_v}{\alpha}\left[\frac{P}{H} - \tau_{max}(L - x_1)\right]\left(\frac{e^{\alpha x} - e^{-\alpha x}}{e^{\alpha x_1} + e^{-\alpha x_1}}\right) \tag{37}$$

The shear stress throughout the interface from x=0 to $x=x_1$ is given by:

$$\tau(x) = k_s \delta_s(x) \tag{38}$$

From $x=x_1$ to x=L the shear stress is given by:

$$\tau(x) = \tau_{max} = c \tag{39}$$

The x_1 point is obtained iteratively as proposed by Hird and Russell (1990), solving the following equation (Table 4 provides this value for different load level P by applying the Newton Raphson iterative scheme):

$$\left(\frac{e^{\alpha x_1} - e^{-\alpha x_1}}{e^{\alpha x_1} + e^{-\alpha x_1}}\right) + \alpha(L - x_1) - \frac{P\alpha}{\tau_{max} H} = 0 \tag{40}$$

Table 4. Definition of x_1 point

P(kN)	x_1 (m)
95.2089(*)	10.0
100	9.842
200	6.595
300	3.794
400	2.103

(*) load level lower than 95.2089kN does not lead to a maximal shear stress

An initial normal stress (0.1kPa) was applied to the interface elements in order to maintain them under compression stress state. This stress state doesn't influence the response because the interface is considered purely cohesive ($\phi=\psi=0^o$). Figure 13 presents the shear stress through the interface for various force levels using Gauss-Legendre numerical integration. Good agreement is observed between the numerical and analytical results.

Figure 14 presents the distribution of the horizontal displacement along the block for different load levels. Good agreement is observed between the numerical results obtained in this work and the numerical results presented by Hird and Russel (1990).

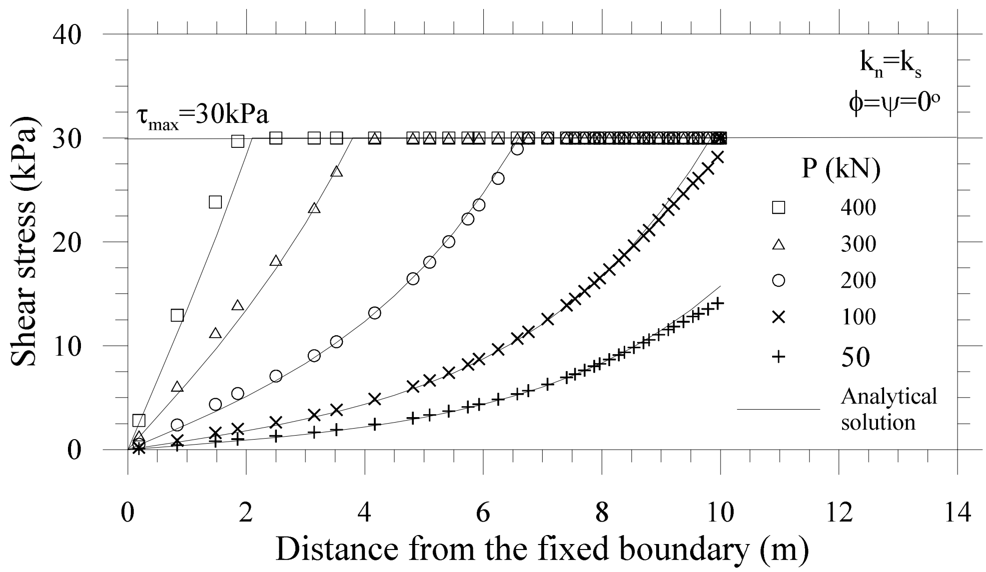

Figure 13. Shear stress through the interface - k_n=k_s e ϕ=ψ=0^o

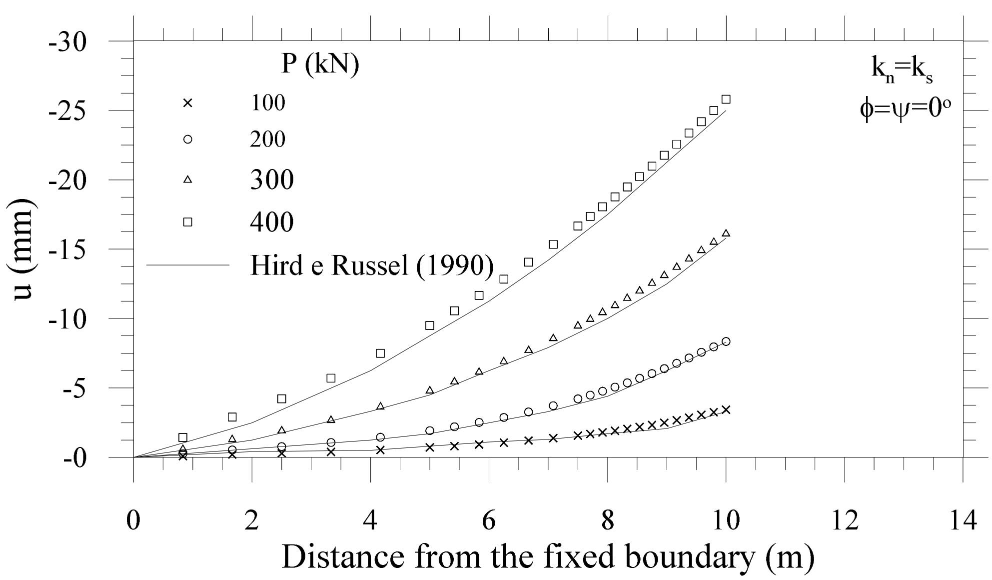

Figure 14. Block horizontal displacement distribution - k_n=k_s e ϕ=ψ=0^o

4 CONCLUSIONS

This paper presented the null thickness interface elements implemented into ANLOG software to be used on static analysis of mechanical problems in axi-symmetric and plane strain conditions mechanical. The following conclusion can be drawn:

1. The implementation is verified when compared to some analytical problems.

2. The kinetic inconsistency and oscillatory behavior on the shear stress through the interface, observed by many authors in the literature, depend on the loading condition. Some loading conditions provides a oscillatory behavior in terms of the shear stress but are self-balanced and do not lead a problem when used in a finite element mesh with other plane elements.

3. In the case of a smooth interface a non-associated ($\phi \neq \psi$) elastoplastic model must be used to guarantee no dilatation on the interface.

4. The interface dilatancy angle ψ does not influence the maximal shear stress level but it influences the normal relative displacement that could be null if this angle is done null.

ACKNOWLEDGEMENTS

The authors are grateful for the financial support received from CAPES, CNPq, FAPEMIG, Fundação Gorceix, PPGEM/UFOP, PROPEC/UFOP, PROPP/UFOP. The first author is grateful for the grant received by CAPES. The second author is grateful for the grant received by FAPEMIG. They also acknowledge Prof. John P. White for the editorial review of this text.

REFERENCES

Beer, G., 1985. An isoparametric joint-interface element for finite element analysis. *International Journal for Numerical Methods in Engineering* - 21, 585-600.

Boulon, M., Garnica, P., & Vermeer, P. A., 1995. Soil-structure interaction: FEM computations. *Mechanics of Geomaterial Interface*. Edt.by A.P.S. Selvadurai and M.J.Boulon, p.147-171.

Bouzid, D. A., Tiliouine, B., & Vermeer, P. A., 2004. Exact formulation of interface stiffness matrix for axi-symmetric bodies under non-axi-symmetric loading. *Computers and Geotechnics*, 31, 75-87.

Brocklehurst, C. J., 1993. *Finite element studies of reinforced and unreinforced two-layer soil system*. PhD. Thesis, University of Oxford.

Coutinho, A. L. G. A., Martins, A. D., Sydenstricker R. M., Alves J. L. D. & Landau L., 2003. Simple zero thickness kinematically consistent interface elements. *Computers and Geotechnics*, v. 30, Issue 5, July 2003, p. 347-374.

Day, R. A., & Potts, D. M., 1994. Zero thickness interface elements – numerical stability and application. *International Journal for Numerical and Analytical Methods in Geomechanics*, v.18, p. 689-708.

Day, R. A., & Potts, D. M., 1998. The efect of interfaces properties on retaining walls behavior. *International Journal for Numerical and Analytical Methods in Geomechanics*, v.22, p.1021-1033.

Desai, C.S., Zaman, M.M., Lightner, J.G., & Siriwardane, H.J., 1984. Thin-layer element for interfaces and joints. *International Journal for Numerical and Analytical Methods in Geomechanics*, v.8, p.19-43.

Gens, A., Carol, I., & Alonso, E.E., 1989. An interface element formulation for the analysis of soil-reinforcement interaction. *Computer and Geotechnics*, v.7, p.133-151.

Gens, A., Carol, I., & Alonso, E.E., 1995. Rock joints: FEM implementation and applications. *Mechanics of Geomaterial Interface*. Edt.by A.P.S. Selvadurai and M.J.Boulon, p.395-420.

Ghaboussi,J., Wilson, E. L., & Isenberg, J., 1973. Finite element for rock joints and interfaces. *Journal of Soil Mechanics and Foundation Division*, v.99(10), p.833-848.

Goodman, R. E., Taylor, R. L., & Brekke, T. L., 1968. A model for the mechanics of Jointed Rock. *Journal soil Mechanics and Foundation Division*, ASCE, v.94, SM3, p.637-659.

Herrmann, L.R., 1978. Finite element analysis of contact problems. *Journal of the engineering mechanics division*, EM5, p.1043-1057.

Heuze, F. E., & Barbour, T. G., 1882. New models for rock joints and interfaces. *Journal Geotechnical Engineering*, ASCE, v.108(5), p.757-776.

Hird, C. C. & Russell, D., 1990. A benchmark for soil-structure interface elements. *Computers and Geotechnics*, v.10(2), p.139-147.

Kaliakin, V. N., & Li, J., 1995. Insight into deficiencies associated with commonly used zero-thickness interface elements. *Computers and Geotechnics*, v.17, p.225-252.

Lei, X., 2001. Contact friction analysis with a simple interface element. *Computer methods in applied mechanics and engineering*, v.190, p.1955-1965.

Mao, J., 2004. A finite element approach to solve contact problems in geotechnical engineering. *International Journal for Numerical and Analytical Methods in Geomechanics*, v.29, p.525-550.

Nogueira, C. L. (1998). *Análise Não Linear de Escavações e Aterros*. PhD thesis, Curso de Pós-Graduação em Engenharia da Pontifícia Universidade Católica do Rio de Janeiro PUC/Rio.

Nogueira, C. L. (2010*). Manual de Utilização do ANLOG*

Oliveira, R. R. V., 2006. *Análise Elastoplástica via MEF de Problemas em Solos Reforçados*. Dissertação de mestrado. PROPEC/UFOP (in Portuguese)

Oliveira, R.R.V., Nogueira, C.L., Araújo, L.G., Faria, P. O., 2005. Modelo numérico via MEF para análise elastoplástica de problemas axissimétricos em solos reforçados. *XXV IIberian Latin American Congress on Computational Methods in Engineering*. Vitória, ES, v. único. p. 1-15.

Pande, G. N., & Shama, K. G., 1979. On joint/interface elements and associated problems of numerical ill-conditioning. *International Journal for Numerical and Analytical Methods in Geomechanics*, v.3, p.293-300.

Pereira, A. R., 2003. *Análise Não Linear Física de Estruturas de Solos Reforçados*. Dissertação de mestrado. PROPEC/UFOP. (in Portuguese)

Plesha, M. E., 1987. Constitutive models for rock discontinuites with dilatancy and surface degradation. *International Journal for Numerical and Analytical Methods in Geomechanics*, v.11, p.345-362.

Schellekens,J.C.J. & De Borst, R., 1993. On the numerical integration of interface elements. *International Journal for numerical methods in engineering*, v.36, p.43-66.

Simão, J.T. (2014) *Um modelo numérico para análise elastoplástica de maciços rochosos com base no critério de ruptura de Hoek-Brown*. Dissertação de Mestrado, PPGEM/EM/UFOP, 90p.

Sugimoto, M. & Alagiyawanna, A.M.N., 2003. Pullout behavior of geogrid by test and numerical analysis. *Journal Geotechnical and Geoenvironmental Engineering*, ASCE, april, p.361-371.

Wang, X., & Wang, L.B., 2006. Continuous interface elements subject to large shear deformations. *International Journal of Geomechanics*, ASCE, march-april, p.97-107.

Wang, Z., & Wang, R., 2002. A study of soil-reinforcement interface friction. *Journal Geotechnical and Geoenvironmental Engineering*, ASCE, january, p.92-94.